

# Step-flow growth of nanolaminate $\text{Ti}_3\text{SiC}_2$ epitaxial layers on 4H-SiC(0 0 0 1)

Kristina Buchholt, Per Eklund, Jens Jensen, Jun Lu, Anita Lloyd Spetz and Lars Hultman

**Linköping University Post Print**

N.B.: When citing this work, cite the original article.

Original Publication:

Kristina Buchholt, Per Eklund, Jens Jensen, Jun Lu, Anita Lloyd Spetz and Lars Hultman, Step-flow growth of nanolaminate  $\text{Ti}_3\text{SiC}_2$  epitaxial layers on 4H-SiC(0 0 0 1), 2011, SCRIPTA MATERIALIA, (64), 12, 1141-1144.

<http://dx.doi.org/10.1016/j.scriptamat.2011.03.013>

Copyright: Elsevier Science B.V., Amsterdam.

<http://www.elsevier.com/>

Postprint available at: Linköping University Electronic Press

<http://urn.kb.se/resolve?urn=urn:nbn:se:liu:diva-68684>

# Step-Flow Growth of Nanolaminate $\text{Ti}_3\text{SiC}_2$ Epitaxial Layers on 4H-SiC(0001)

Kristina Buchholt\*, Per Eklund, Jens Jensen, Jun Lu, Anita Lloyd Spetz, and Lars Hultman

*Department of Physics, Chemistry and Biology, IFM, Linköping University, 581 83 Linköping, Sweden*

Epitaxial  $\text{Ti}_3\text{SiC}_2(0001)$  films were deposited on  $4^\circ$  off-cut 4H-SiC(0001) wafers using magnetron sputtering. A lateral step-flow growth mechanism of the  $\text{Ti}_3\text{SiC}_2$  was discovered by X-ray diffraction, elastic recoil detection analysis, atomic force microscopy, and electron microscopy. Helium ion microscopy revealed contrast variations on the  $\text{Ti}_3\text{SiC}_2$  terraces, suggesting a mixed Si and Ti(C) termination. Si-rich growth conditions results in  $\text{Ti}_3\text{SiC}_2$  layers with pronounced  $\{11\bar{2}0\}$  faceting and off-oriented  $\text{TiSi}_2$  crystallites, while stoichiometric growth yields truncated  $\{1\bar{1}00\}$  terrace edges.

*Keywords:* Sputtering, atomic force microscopy (AFM), helium ion microscopy (HIM), transmission electron microscopy (TEM), crystal structure

---

\* Corresponding author. Tel.: +46 13281062;  
e-mail: kribu@ifm.liu.se.

Silicon carbide (SiC) is a wide bandgap semiconductor with high breakdown field and high thermal conductivity; it therefore finds applications in devices and sensors for operation at high power and high temperature [1-4]. In such electronic device applications, a challenge is the formation of ohmic contacts to the SiC, as well as the durability of the contacts when operated at elevated temperatures. High-temperature annealed Ti/Al contacts on p-type SiC have been reported to form  $\text{Ti}_3\text{SiC}_2$  [5-8], which is suggested to contribute to the ohmic behavior of the contacts [9-11]. Formation of  $\text{Ti}_3\text{SiC}_2$  and subsequent ohmic behavior has also been reported for high-temperature annealed Ti-based contacts on n-type SiC [12, 13].

$\text{Ti}_3\text{SiC}_2$  is an inherently nanolaminated material that combines metallic properties such as high thermal and electrical conductivity with ceramic properties like being resistant to thermal shock [14, 15]. Furthermore,  $\text{Ti}_3\text{SiC}_2$  and 4H-SiC are tie-line phases with a relatively good lattice match of the basal planes. Thus,  $\text{Ti}_3\text{SiC}_2$  is an interesting ohmic contact material to SiC, and since epitaxial growth by direct deposition of  $\text{Ti}_3\text{SiC}_2$  onto SiC using vapor deposition offers more control than annealing, it is a promising technique for easier realization of an ordered and stable structure.

We have reported elsewhere [16] that epitaxially grown  $\text{Ti}_3\text{SiC}_2$  can form ohmic contacts to n-type 4H-SiC. The chemical nature and morphology of  $\text{Ti}_3\text{SiC}_2(0001)$  layers on SiC is, however, not known, but are likely factors influencing the ohmic contact formation to SiC. Emmerlich et al. reported the synthesis of epitaxial  $\text{Ti}_3\text{SiC}_2(0001)$  thin films using DC magnetron sputtering from three sources onto on-axis  $\text{MgO}(111)$  and  $\text{Al}_2\text{O}_3(0001)$  substrates, and suggested that  $\text{Ti}_3\text{SiC}_2$  grows in a step-flow mode where the steps on the surface are provided by threading screw dislocations [17].

Here, we investigate the growth of  $\text{Ti}_3\text{SiC}_2$  thin films on  $4^\circ$  off-cut 4H-SiC using DC magnetron sputtering from three sources. We find that the  $\text{Ti}_3\text{SiC}_2$  grows epitaxially by a step-flow mechanism determined by the existing surface steps of the SiC substrate, in the absence of screw dislocations. The  $\text{Ti}_3\text{SiC}_2$  layers exhibits a mixture of half, full, and multiple unit cell high steps. Si-supersaturation growth conditions results in growth of steps with  $\{11\bar{2}0\}$  faceting, while stoichiometric conditions yield  $\{1\bar{1}00\}$  step truncation. Helium ion microscopy studies reveal differently terminated terraces.

4H-SiC(0001) wafers, n-type, Si-face,  $4^\circ$  off-cut, from SiCrystal [18], were used as substrates. The micropipe density of the wafers is  $<10\text{ cm}^{-2}$ . On top of the 4H-SiC, epi-layers with Al and N doping atoms for the p- and n-type, respectively, were grown by Acreo [19], using chemical vapor deposition. Prior to deposition, the substrates were ultrasonically cleaned in acetone and isopropanol for 5 minutes each. The substrates were then blown dry in  $\text{N}_2$  gas and immediately loaded into the ultra-high vacuum magnetron sputtering system. The substrates were heated to the deposition temperature of  $800^\circ\text{C}$ , and left to stabilize at that temperature for 1 h. Immediately before deposition the substrates were plasma etched for 30 minutes to remove any surface oxide on the SiC. Plasma etching was performed through operating the Ti-target at 25 mA in high purity Ar discharges, while applying a negative bias of -50 V to the substrate. The  $\text{Ti}_3\text{SiC}_2$  films were grown using high purity C, Si, and Ti targets as described elsewhere [17, 20], with the difference of a 50 mm Si target being used for our experiments, instead of a 25 mm target. All depositions were performed at a constant pressure of  $\sim 0.5\text{ Pa}$  in high purity Ar discharges. The magnetrons were operated in current-regulation mode, (voltages given in parenthesis), with the target currents fixed at 310 mA (330 V) for Ti, and 360

mA (580 V) for C. The Si-target current was varied between 80 mA (380 V) and 160 mA (440 V) in order to investigate the influence of the Si content on the growth of the  $\text{Ti}_3\text{SiC}_2$  phase. 1 h long depositions were performed resulting in films approximately 200 nm thick.

As-deposited films were characterized by  $\theta$ -2 $\theta$  X-ray diffraction (XRD) measurements, performed in a Philips PW 1820 diffractometer with Cu  $K\alpha$  radiation, operated at 40 kV and 40 mA. The instrument was aligned using the (0004) SiC substrate peak giving an offset of  $\sim 4^\circ$  due to the SiC substrate being cut  $4^\circ$  off axis. Surface morphology was investigated using secondary-electron images from a Leo 1550 Gemini scanning electron microscope (SEM), using a 5 kV accelerating voltage, and helium ion microscopy (HIM), using an ORION PLUS microscope from Carl Zeiss SMT. Plan-view images were obtained using 30 keV  $\text{He}^+$  ions. The imaging was performed by detecting secondary electrons, using an Everhart-Thornley detector. Prior to observation the sample was plasma cleaned. A Dimension 3100 atomic force microscopy (AFM), was also used to investigate surface morphology. Cross-sectional samples for transmission electron microscopy (TEM) using a Tecnai G2 TF20UT FEG, were prepared using standard preparation methods. Elemental depth profiles of the as-deposited films were performed using time-of-flight elastic recoil detection analysis (ToF-ERDA). Here, a 40 MeV  $^{127}\text{I}^{9+}$  beam was directed to the films at an incident angle of  $67.5^\circ$  with respect to the surface normal, and the recoils were detected at an angle of  $45^\circ$  [21, 22].

Figure 1 (a) and (b) show XRD patterns from  $\text{Ti}_3\text{SiC}_2$  films deposited with Si currents of 80 mA and 160 mA, respectively. The film deposited with 80 mA Si current shows only (0001)  $\text{Ti}_3\text{SiC}_2$  diffraction peaks while the pattern from the 160 mA sample also contains peaks originating from C49- $\text{TiSi}_2$  (ICDD PDF 40-1132 and

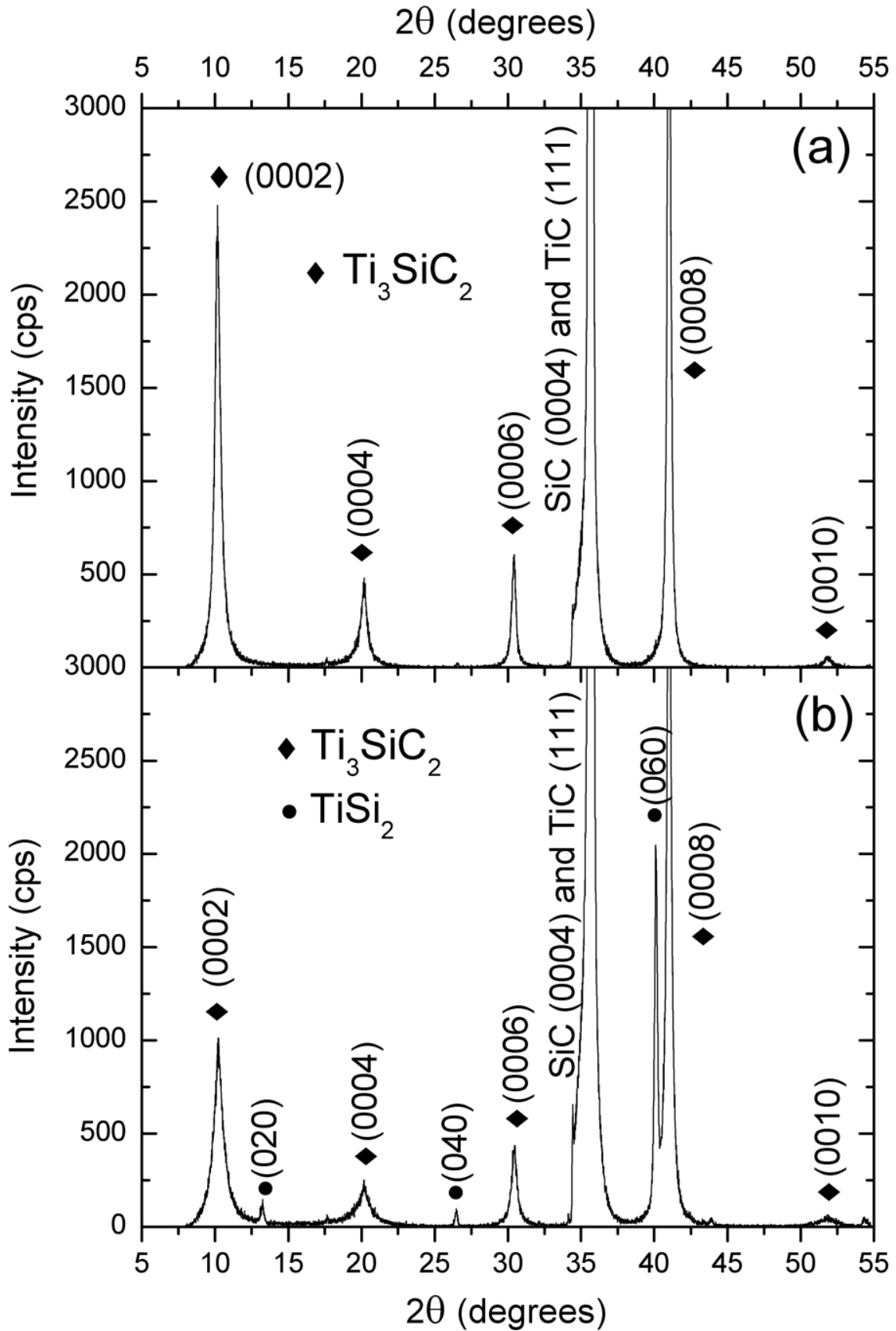


**Figure 1.** XRD patterns from  $\text{Ti}_3\text{SiC}_2$  films grown with (a) 80 and (b) 160 mA Si target current.

10-0225 for  $\text{Ti}_3\text{SiC}_2$  and  $\text{TiSi}_2$ , respectively). However, the presence of small amounts of TiC in the samples can not be ruled out using XRD since the SiC (0004) substrate peak overlaps with the TiC (111) peak (PDF 22-1317 and 32-1383 for SiC and TiC, respectively). Also, due to the limitations of XRD when analyzing thin films, other minority phases might not be detected. The presence of only (0001) diffraction peaks indicates that the  $\text{Ti}_3\text{SiC}_2$  films are (0001) oriented on the 4H-SiC(0001) substrate with a  $4^\circ$  angle relative to the substrate surface, following the substrate  $4^\circ$  off cut angle.

Using ERDA depth profiling, the composition of the 80 mA sample was determined to be 48 at. % Ti, 16 at. % Si, and 36 at. % C. The 160 mA sample has the composition of 39 at. % Ti, 33 at. % Si, and 28 at. % C. Assuming a film composition with  $\text{Ti}_3\text{SiC}_2$  and  $\text{TiSi}_2$  present, as was seen in XRD for the 160 mA sample, this leaves 10 at. % C unaccounted for. An explanation for this could be substoichiometry of Si in the  $\text{Ti}_3\text{SiC}_2$  phase.  $\text{Ti}_3\text{Si}_x\text{C}_2$ , with  $x < 1$ , has been reported for Cu-coated  $\text{Ti}_3\text{SiC}_2$  at elevated temperatures by the de-intercalation of Si [23], and first principle calculations for the related material  $\text{Ti}_2\text{AlC}$  show that the material is stable down to a composition of  $\text{Ti}_2\text{Al}_{0.5}\text{C}$  [24]. Another possible explanation is the presence of small amounts of TiC in the film. For both samples, oxygen was only found at the surface of the  $\text{Ti}_3\text{SiC}_2$  films; no oxygen was found throughout the films or at the interface between the SiC and the  $\text{Ti}_3\text{SiC}_2$ . The absence of oxygen at the interface shows that the plasma etching made before deposition is successful in removing the native oxide of the SiC substrate, which is important since interfacial oxygen has a detrimental effect both on the specific contact resistance, and the stability of ohmic contacts.

Figure 2(a) and (b) show SEM images of the 80 mA and 160 mA samples, respectively. The films are seen to consist of stacked plate-shaped  $\text{Ti}_3\text{SiC}_2$  layers. The

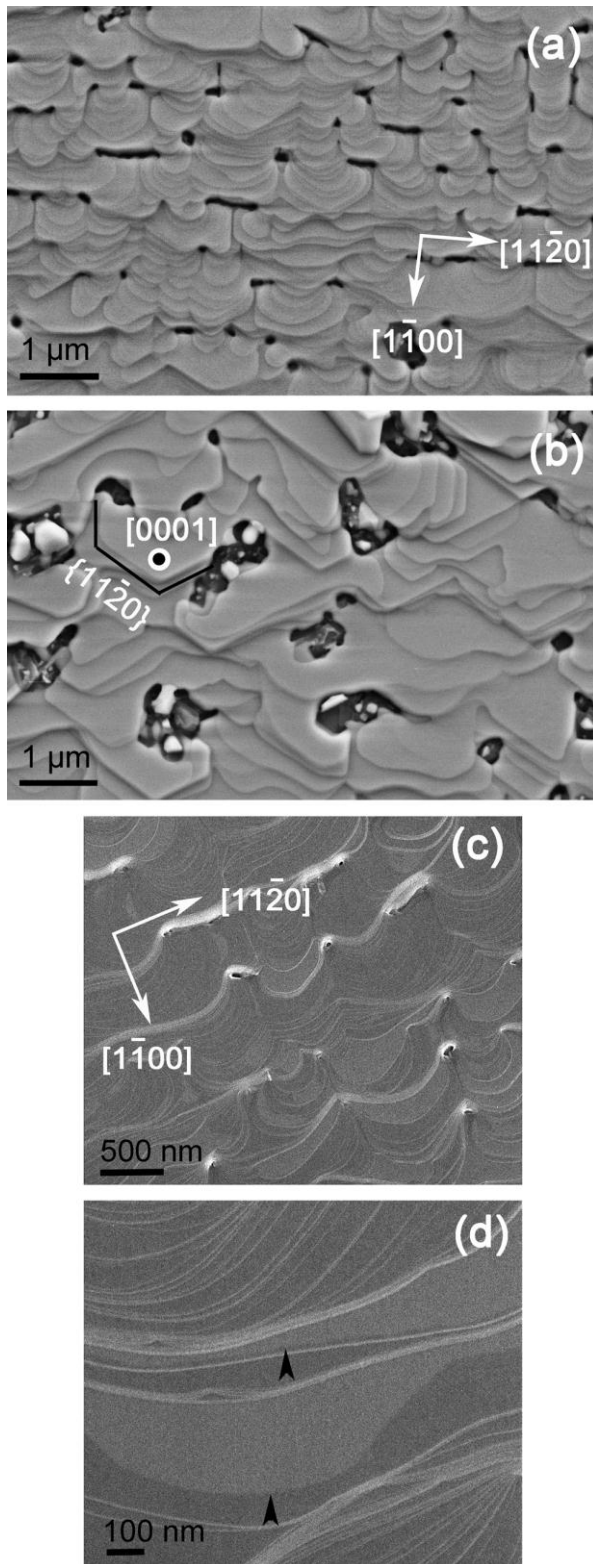


**Figure 2.** SEM images of the films with (a) 80, and (b) 160 mA Si current. The SiC substrate surface step normal  $[1\bar{1}00]$ , and  $\text{Ti}_3\text{SiC}_2$  step facets  $\{11\bar{2}0\}$ , are indicated. HIM images of the 80 mA sample, (c) overview, and (d) higher magnification. Arrowheads point to a transition in contrast from dark to bright on terraces.

higher Si-content sample in addition exhibits holes in the plate-shaped  $\text{Ti}_3\text{SiC}_2$  layers in which polyhedral grains have grown as described below. The off cut of the SiC substrate provides growth steps for the  $\text{Ti}_3\text{SiC}_2$ . This is in contrast to nucleation of  $\text{Ti}_3\text{SiC}_2$  assisted by threading screw dislocations, as observed for growth of  $\text{Ti}_3\text{SiC}_2$  on  $\text{Al}_2\text{O}_3(0001)$  [17].

The  $\text{Ti}_3\text{SiC}_2$  layers attain a close to perfect hexagonal growth pattern of low-energy  $\{11\bar{2}0\}$  step facets under Si-rich growth conditions (the 160 mA sample). For stoichiometric conditions (80 mA sample), however, the growth steps are rounded from  $\{1\bar{1}00\}$  truncation. These results indicate that Si supersaturation is required to maintain equilibrium-shape steps. A reason for this may be the relatively weak bonding of Si in the  $\text{Ti}_3\text{SiC}_2$  and its tendency to leave the crystal on the exposed  $a$  planes [25]. Further support of this reasoning is the known fact that substantial Si supersaturation is required to nucleate  $\text{Ti}_3\text{SiC}_2$  in thin film growth experiments [17, 26]. It is therefore reasonable that also the crystal shape can be influenced by the Si content.

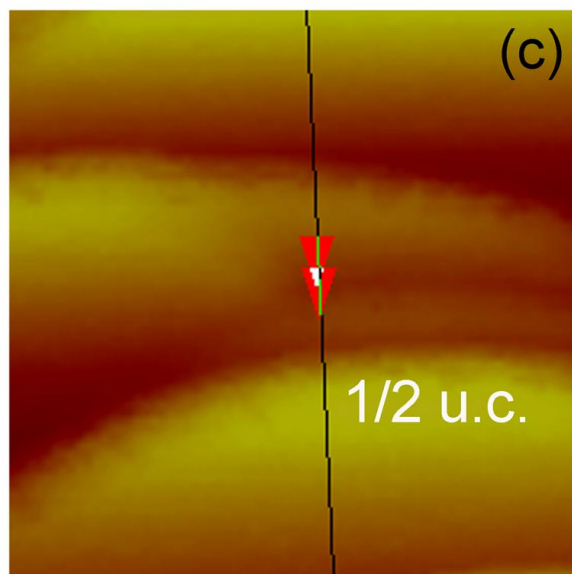
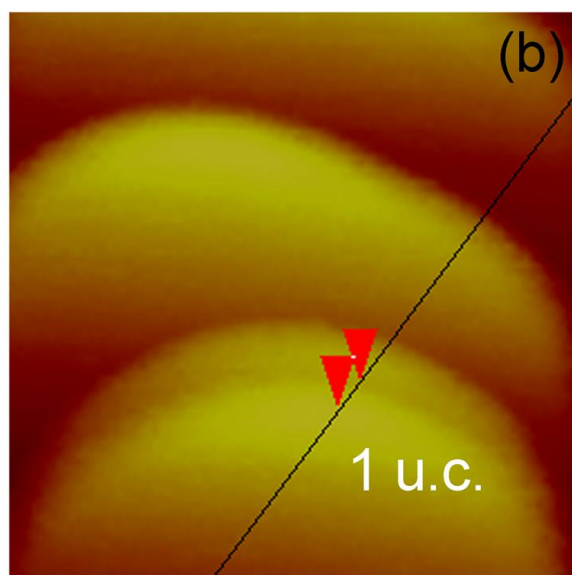
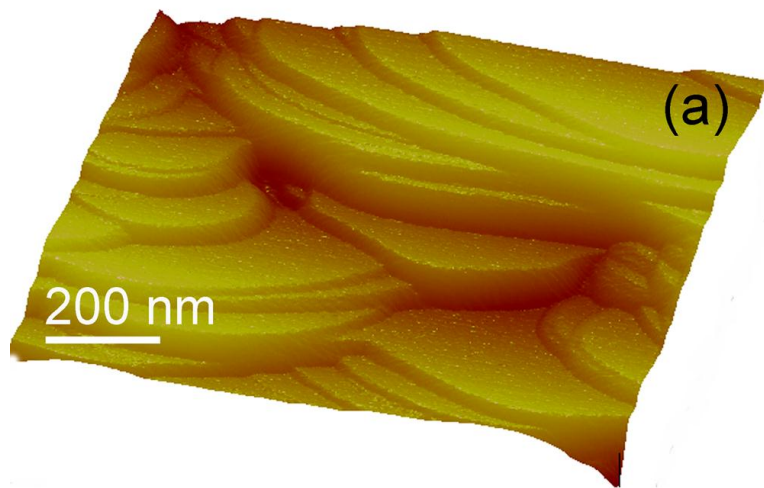
The surface morphology of the 80 mA sample was also investigated using helium ion microscopy (HIM). Primary benefits of the HIM are a smaller probe size and smaller sample interaction volume in the sample, as compared to electrons in a SEM, allowing for significantly higher image resolution. In addition, it has an enhanced surface sensitivity, the secondary electron yield is higher providing a better elemental contrast, and the depth of focus is larger. The images thus provide more detailed information on sample topography and material contrast as compared to SEM imaging [27-29]. The HIM images in Figure 2(c) and (d) show that each of the plateaus in the SEM image actually consists of several terraces. Noteworthy is also the variation in contrast seen on some of the terraces, indicated by arrowheads in

Figure 2(d). This contrast variation may be due to differences in surface chemistry, caused by differences in surface termination affecting the secondary electron yield, corresponding to Si- and Ti- termination, as expected for half and full unit cells of  $\text{Ti}_3\text{SiC}_2$ .

The nature of the terraces was further investigated using atomic force microscopy (AFM). The lattice parameters of  $\text{Ti}_3\text{SiC}_2$  are  $a= 3.062 \text{ \AA}$ , and  $c= 17.637 \text{ \AA}$ , and it belongs to the space group  $\text{P6}_3/\text{mmc}$  (ICDD PDF 40-1132). 4H-SiC has the lattice parameters  $a=3.073 \text{ \AA}$ , and  $c=10.053 \text{ \AA}$ , and belongs to the space group  $\text{P6}_3\text{mc}$  (ICDD PDF 22-1317). This means that  $\text{Ti}_3\text{SiC}_2$  and 4H-SiC both have a hexagonal crystal unit cell with a very small mismatch between the basal planes of less than 0.4 % [8, 14]. Figure 3(a) displays a surface plot of the 80 mA sample. We observe flat terraces and distinct surface steps where the step heights are approximately one unit cell ( $\sim 18 \text{ \AA}$ ), half a unit cell ( $\sim 9 \text{ \AA}$ ), or multiples thereof. Figure 3(b) is a magnification where the step height measured is one unit cell, while Figure 3(c) displays half a unit cell high step.

Our observations of surface terraces with steps that are one-, or half-, a unit cell high are consistent with the findings of Emmerlich et al. for the epitaxial growth of  $\text{Ti}_3\text{SiC}_2$  on  $\text{MgO}(111)$  substrates [17]. The ideal shape of a  $\text{Ti}_3\text{SiC}_2$  crystal is a flat hexagonal prism with six  $\{11\bar{2}0\}$  side faces and two  $\{0001\}$  basal faces [30, 31]. This agrees with the  $\{0001\}$  morphology with  $\{11\bar{2}0\}$  step facets that we observe in XRD and in the SEM images of our samples, as well as observations by Tsukimoto et al. [9], on  $\text{Ti}_3\text{SiC}_2$  layers formed by high-temperature annealing of TiAl-based ohmic contacts on 4H-SiC.

The nature of the grains situated in holes of the plate-shaped layers in the 160 mA sample (see Figure 2(b)), was investigated using transmission electron



**Figure 3.** AFM images from the 80 mA sample, (a) surface plot, (b) 1 unit cell high step, (c)  $\frac{1}{2}$  unit cell high step.

microscopy. Figure 4 shows a cross-sectional TEM image with selected area electron diffraction pattern insets. As can be seen  $\text{Ti}_3\text{SiC}_2$  co-exists with  $\text{TiSi}_2$  grains in the 160 mA samples, consistent with XRD. The diffraction patterns reveal the following epitaxial relationships between the phases:

$(020)\text{TiSi}_2 // (0001)\text{Ti}_3\text{SiC}_2 // (0001)\text{SiC}$ , and

$[202]\text{TiSi}_2 // [1\bar{1}00]\text{Ti}_3\text{SiC}_2 // [1\bar{1}00]\text{SiC}$

Thus, deposition of films during Si supersaturation growth conditions does not prevent the growth of the  $\text{Ti}_3\text{SiC}_2$ , but triggers the nucleation and growth of  $\text{TiSi}_2$ , as well as influences the  $\text{Ti}_3\text{SiC}_2(0001)$  layer termination.

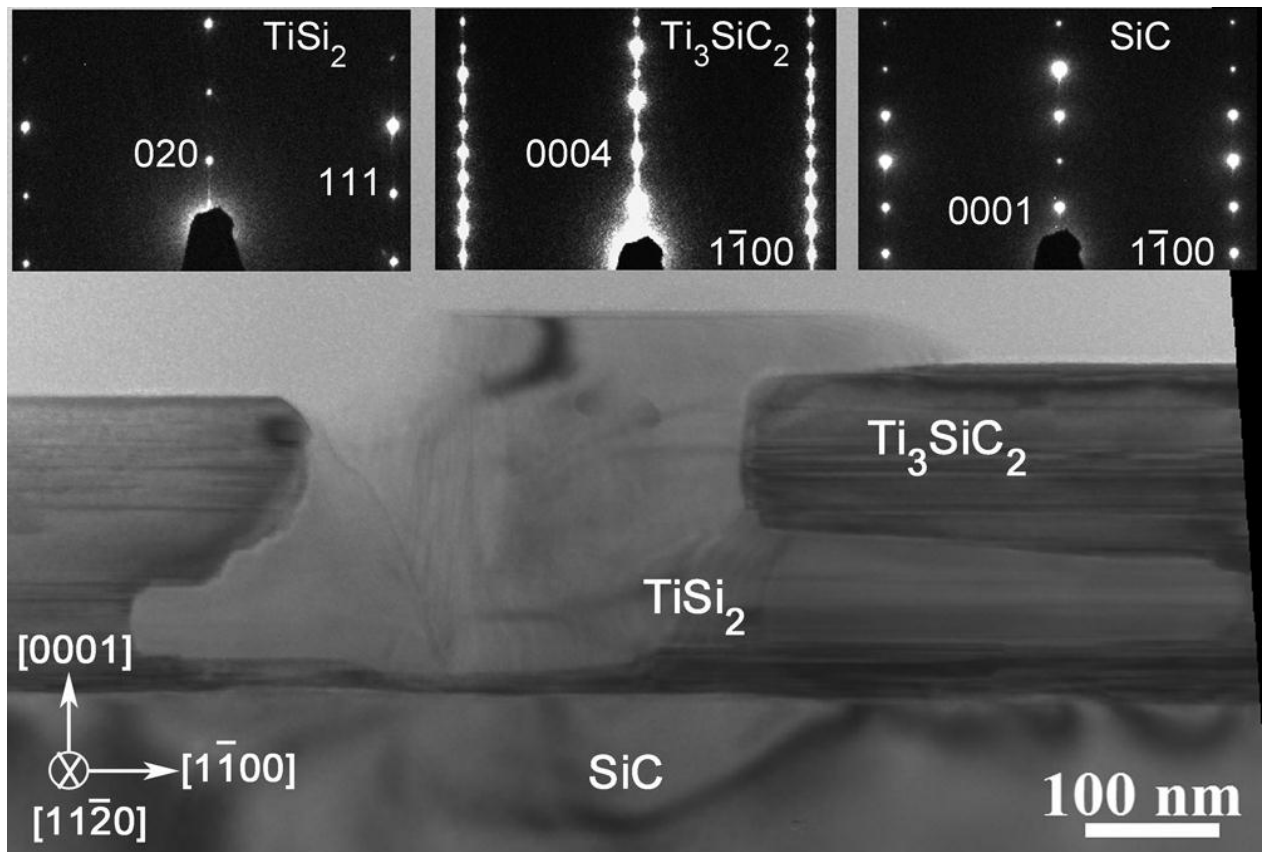


**Figure 4.** Cross-sectional TEM image of the 160 mA sample with selected area electron diffraction pattern insets from SiC,  $\text{TiSi}_2$ , and  $\text{Ti}_3\text{SiC}_2$ .

In summary, we have grown epitaxial  $\text{Ti}_3\text{SiC}_2$  films on  $4^\circ$  off-cut 4H-SiC(0001) using the direct deposition method of DC magnetron sputtering from three separate targets. The growth mode of  $\text{Ti}_3\text{SiC}_2$  epitaxial layers is lateral step-flow with

the propagation of (0001) terraces. Step heights of the terraces are half, one or several unit cells high. Stoichiometric growth conditions lead to phase pure  $\text{Ti}_3\text{SiC}_2$  films with rounded steps caused by  $\{1\bar{1}00\}$  step truncation. Si supersaturation growth conditions, on the other hand, yield a more hexagonal growth pattern of the  $\text{Ti}_3\text{SiC}_2$  with  $\{11\bar{2}0\}$  step faceting, along with the formation of  $\text{TiSi}_2$  grains. Hence, varying the amount of Si present during growth is a means for controlling the morphology of the  $\text{Ti}_3\text{SiC}_2$  layers. Helium ion microscopy investigation of the  $\text{Ti}_3\text{SiC}_2$  layers revealed a contrast variation between the inner and outer parts of the terraces, consistent with the presence of half and full unit cells of  $\text{Ti}_3\text{SiC}_2$  with Si and Ti termination, respectively.

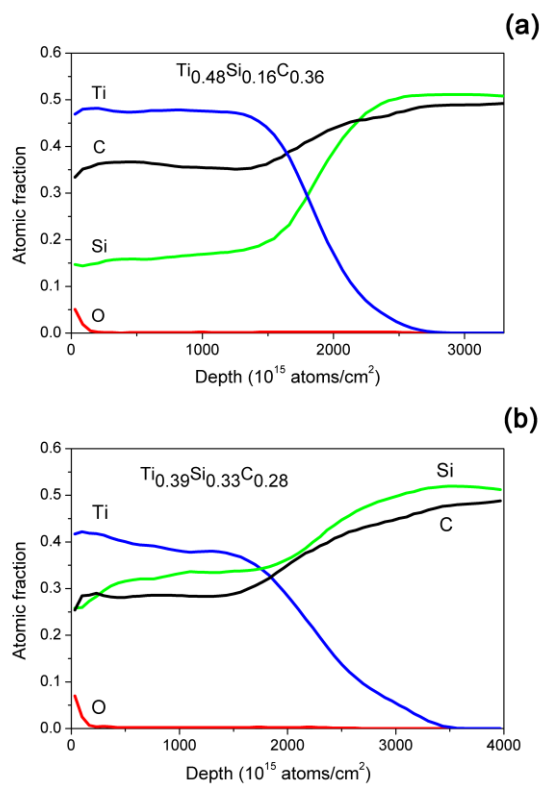
Funding from the VINN Excellence Center in Research and Innovation on Functional Nanoscale Materials (FunMat) by the Swedish Governmental Agency for Innovation Systems is acknowledged. We thank the staff at the Tandem Laboratory, Uppsala University, for support during the ERD analysis, and Dr. F. Pérez-Williard at Carl Zeiss SMT AG, Germany, for helping with HIM observations.

- [1] N. Kondrath, M.K. Kazimierczuk, *Int. J. Electron. Telecom.* 56 (2010) 231.
- [2] S. Leone, F.C. Beyer, A. Henry, C. Hemmingsson, O. Kordina, E. Janzén, *Cryst. Growth Des.* 10 (2010) 3743.
- [3] N.G. Wright, A.B. Horsfall, *J. Phys. D: Appl. Phys.* 40 (2007) 6345.
- [4] S. Leone, F.C. Beyer, H. Pedersen, O. Kordina, A. Henry, E. Janzén, *Cryst. Growth Des.* 10 (2010) 5334.
- [5] B. Pécz, L. Tóth, M.A. di Forte-Poisson, J. Vacas, *Appl. Surf. Sci.* 206 (2003) 8.

- [6] F.A. Mohammad, Y. Cao, K.-C. Chang, L.M. Porter, *Jpn. J. Appl. Phys.* 44 (2005) 5933.
- [7] R. Konishi, R. Yasukochi, O. Nakatsuka, Y. Koide, M. Moriyama, M. Murakami, *Mater. Sci. Eng., B.* 98 (2002) 286.
- [8] S. Tsukimoto, K. Nitta, T. Sakai, M. Moriyama, M. Murakami, *J. Electron. Mater.* 33 (2004) 460.
- [9] S. Tsukimoto, K. Ito, Z. Wang, M. Saito, Y. Ikuhara, M. Murakami, *Mater. Trans.* 50 (2009) 1071.
- [10] Z. Wang, S. Tsukimoto, M. Saito, K. Ito, M. Murakami, Y. Ikuhara, *Phys. Rev. B.* 80 (2009) 245303:1.
- [11] M. Gao, S. Tsukimoto, S.H. Goss, S.P. Tumakha, T. Onishi, M. Murakami, L.J. Brillson, *J. Electron. Mater.* 36 (2007) 277.
- [12] F. Goesmann, R. Schmid-Fetzer, *Semicond. Sci. Technol.* 10 (1995) 1652.
- [13] F. La Via, F. Roccaforte, A. Makhtari, V. Raineri, P. Musumeci, L. Calcagno, *Microelectron. Eng.* 60 (2002) 269.
- [14] M. W. Barsoum, *Prog. Solid St. Chem.* 28 (2000) 201.
- [15] P. Eklund, M. Beckers, U. Jansson, H. Högberg, L. Hultman, *Thin Solid Films* 518 (2010) 1851.
- [16] K. Buchholt, R. Ghandi, M. Domeij, C.M. Zetterling, J. Lu, P. Eklund, L. Hultman, A. Lloyd Spetz, *Appl. Phys. Lett.*, in press.
- [17] J. Emmerlich, H. Högberg, S. Sasvári, P.O.Å. Persson, L. Hultman, *J. Appl. Phys.* 96 (2004) 4817.
- [18] SiCrystal AG, Guenther-Scharowsky-Str.1, D91058 Erlangen, Germany.
- [19] Acreo AB, Electrum 239, 164 40 Kista, Sweden.

- [20] H. Högberg, L. Hultman, J. Emmerlich, T. Joelsson, P. Eklund, J.M. Molina-Aldareguia, J.-P. Palmquist, O. Wilhelmsson, U. Jansson, *Surf. Coat. Technol.* 193 (2005) 6.
- [21] H. J. Whitlow, G. Possnert, C.S. Petersson, *Nucl. Instrum. Methods B.* 27 (1987) 448.
- [22] J. Jensen, D. Martin, A. Surpi, T. Kubart, *Nucl. Instrum. Methods B.* 268 (2010) 1893.
- [23] H. Guo, J. Zhang, F. Li, Y. Liu, J. Yin, Y. J. Zhou, *Eur. Ceram. Soc.* 28 (2008) 2099.
- [24] J. Wang, Y. Zhou, T. Liao, J. Zhang, Z. Lin, *Scr. Mater.* 58 (2008) 227.
- [25] J. Emmerlich, D. Music, P. Eklund, O. Wilhelmsson, U. Jansson, J.M. Schneider, H. Högberg, L. Hultman, *Acta Mater.* 55 (2007) 1479.
- [26] P. Eklund, M. Beckers, J. Frodelius, H. Högberg, L. Hultman, *J. Vac. Sci. Technol. A.* 5 (2007) 1381.
- [27] B.W. Ward, J.A. Notte, N.P. Economou, *J. Vac. Sci. Technol. B.* 24 (2006), , 2871.
- [28] R. Hill, J. Notte, B. Ward, *Phys. Procedia.* 1 (2008) 135.
- [29] D.C. Bell, *Microsc. Microanal.* 15 (2009) 147.
- [30] K. Tang, C. Wang, Y. Huang, Q. Zan, *J. Cryst. Growth.* 222 (2001) 130.
- [31] K. Tang, C. Wang, Y. Huang, X. J. Xu, *Alloys Compd.* 329 (2001) 136.

## Supplementary data



Elastic recoil detection analysis (ERDA) depth profiles from the films with (a) 80 mA and (b) 160 mA Si target current. (For color reproduction on the web).